2018

Electron Trapping from Interactions between Laser-Driven Relativistic Plasma Waves

Grigory Golovin
University of Nebraska-Lincoln, ggolovin2@unl.edu

Wenchao Yan
University of Nebraska-Lincoln

Ji Luo
Shanghai Jiaotong University

Colton Fruhling
University of Nebraska - Lincoln, cfruhling2@unl.edu

Daniel Haden
University of Nebraska–Lincoln, daniel.haden@unl.edu

See next page for additional authors

Authors

Grigory Golovin, Wenchao Yan, Ji Luo, Colton Fruhling, Daniel Haden, Baozhen Zhao, Cheng Liu, Min Chen, Shouyuan Chen, Ping Zhang, Sudeep Banerjee, and Donald Umstadter

Electron Trapping from Interactions between Laser-Driven Relativistic Plasma Waves

Grigory Golovin,[1] Wenchao Yan,[1] Ji Luo,[2,3] Colton Fruhling,[1] Dan Haden,[1] Baozhen Zhao,[1] Cheng Liu,[1] Min Chen,[2,3] Shouyuan Chen,[1] Ping Zhang,[1] Sudeep Banerjee,[1] and Donald Umstadter[1,*]

[1]*Department of Physics and Astronomy, University of Nebraska-Lincoln, Lincoln, Nebraska 68588, USA*
[2]*Key Laboratory for Laser Plasmas (Ministry of Education) and School of Physics and Astronomy,*
Shanghai Jiao Tong University, Shanghai 200240, China
[3]*Collaborative Innovation Center of IFSA (CICIFSA), Shanghai Jiao Tong University, Shanghai 200240, China*

Interactions of large-amplitude relativistic plasma waves were investigated experimentally by propagating two synchronized ultraintense femtosecond laser pulses in plasma at oblique crossing angles to each other. The electrostatic and electromagnetic fields of the colliding waves acted to preaccelerate and trap electrons via previously predicted, but untested injection mechanisms of ponderomotive drift and wake-wake interference. High-quality energetic electron beams were produced, also revealing valuable new information about plasma-wave dynamics.

Interactions between relativistic plasma waves are central to plasma physics, astrophysics [1,2], controlled fusion [3], wakefield electron accelerators [4–7], and compact x-ray sources [8,9]. Recently developed capabilities—for driving relativistic transverse electromagnetic plasma waves (referred here simply as laser pulses), and relativistic longitudinal electrostatic wakefield electron plasma waves (referred here as wakes)—have greatly enhanced laboratory studies. The greatest current interest in these waves stems from their remarkably high acceleration gradients (TeV/cm and GeV/cm, respectively). Wakes can be driven either by short-duration laser or charged-particle pulses. Such wakes have been shown to accelerate electrons to >GeV energy in distances of just cm [10] or m [11], respectively. However, for electrons to gain energy from the wake, they must first become trapped by it.

A force must be exerted on an electron to give it the velocity and phase required for trapping, i.e., inject it into the wake. In the case of plasma-based electron accelerators, since the phase velocity of the wake is relativistic, so too is the velocity required for injection. Several mechanisms can be employed to provide the injection force. A propagating wake can self-inject, such as when it breaks [12], or when its wavelength suddenly changes due to defocusing of the wake driver [13], or due to an encounter with a sharp plasma-density gradient [14–16]. Alternatively, the wake driver can liberate and inject new electrons via photoionization [17,18].

The greatest flexibility and control over the injection process can be achieved when the injector is separate from the wake driver. In this case, the phase of the wake into which the electrons are injected can be precisely controlled, resulting in improved accelerator performance with reduced energy spread and beam emittance. If an intense laser pulse is used as the injector (referred as optical injection), it can inject electrons via a time-averaged ponderomotive drift in its steep electromagnetic field gradient [19], photoionization [19–21], or stochastic heating in an optical beat wave [22–29]. Injection can be also caused by interference of overlapping wakes [30–32].

Reported here is the first experimental demonstration of two of these controlled injection mechanisms: ponderomotive drift and wake-wake interference, both of which had originally been proposed theoretically more than two decades ago [19,30]. Two laser pulses (drive and injector) were propagated through plasma obliquely and in crossing directions. Both were focused to sufficiently high intensity levels to drive their own wakes, enabling injection by wake-wake interference. The intensity of the injector pulse (1.7×10^{20} W/cm^2) was several orders of magnitude higher than what was used in prior experiments on beat wave injection [23–29], high enough to cause injection via ponderomotive drift. To eliminate contribution from the competing mechanism of beat wave injection, the delay between when the drive and injector pulses arrived at their intersection was varied over a large range. Injection was observed by measuring the properties of the e beams accelerated in the drive pulse direction. The dependence of these properties on the delay also proved to be a novel diagnostic of wake period and lifetime.

The experiments were performed at the Extreme Light Laboratory, University of Nebraska-Lincoln [33]. After amplification, the laser pulse (800 nm, oscillation period of 2.67 fs) was split into two pulses, which were compressed by independent grating compressors [34]. An $f/14$ parabolic mirror focused the drive pulse (1.2 J, 36 fs) to a 20-μm (FWHM) focal spot, corresponding to normalized vector potential of $a_0 = 1.4$. An $f/2$ parabolic mirror focused the
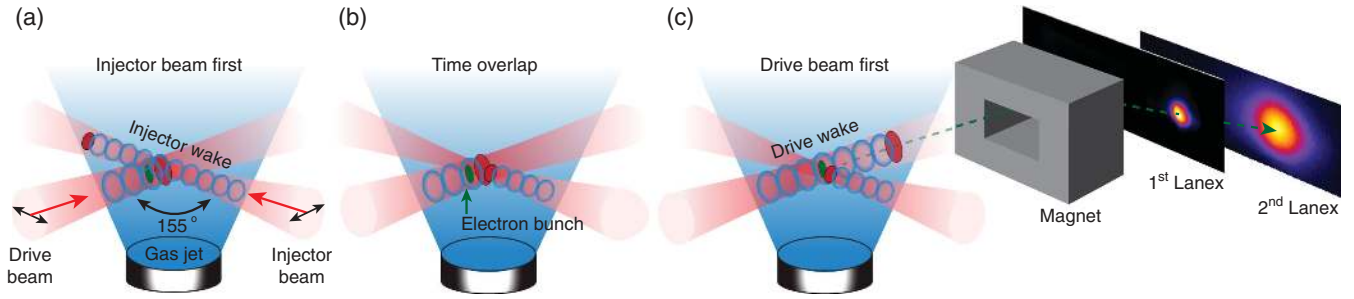
FIG. 1.   Schematic of the experiment. By changing the delay between pulse arrival times, three scenarios resulted: (a) the drive pulse arrives at the intersection after the injector one and interacts with the injector wake. (b) Both pulses arrive at the intersection simultaneously. (c) The injector pulse arrives at the intersection after the drive one and interacts with the drive wake. The polarization of the laser pulses is horizontal (black arrows), with the directions indicated by red arrows.

injector pulse (0.9 J, 34 fs) to a 2.8-μm focal spot, corresponding to intensity of 1.7×10^{20} W/cm^2 ($a_0 \sim 9$). We chose the tight focusing geometry to maximize the injector pulse intensity and access the regime of ponderomotive drift and wake-wake interference injection. Adaptive closed-loop feedback-control systems corrected the spectral phase distortions [35] and spatial aberrations [36] of both pulses. The pulses were polarized in the horizontal plane and intersected at an oblique angle (155°) inside a 2-mm gas jet [37]. Because the ponderomotive force of the injector pulse and the wakefields of the drive pulse are both three dimensional, having comparable longitudinal and transverse components, electrons can be kicked into many different angles and subsequently trapped [19,39]. Thus, the injection mechanisms under study are expected to occur for a wide range of interaction angles. Although it may not have been optimal, the choice of interaction angle used in this experiment was based on the sizes of available optics and working space. An optical delay line adjusted the arrival times of the pulses to their intersection. The e-beam energy spectra were measured using a double-screen (fast Lanex) magnetic spectrometer (0.7-T, 15-cm-long magnet) with 1% energy resolution for 100–300 MeV.

We started with the laser pulses overlapped in time [Fig. 1(b)]. In this scenario, we observed stable, quasimonoenergetic (4% rms spread), few-pC e beams. By varying the plasma density over $(0.65–1.30) \times 10^{19}$ cm^{-3}, the e beams were tuned from 130–170 MeV. With the drive pulse alone, we observed stable, quasimonoenergetic ($\sim$10% rms) e beams, but with 2 orders of magnitude lower charge (80 ± 40 fC based on 20 shots averaging). This single-pulse self-injection is likely due to marginal wave breaking over a short distance. Massive continuous self-injection occurred at higher densities ($>1.30 \times 10^{19}$ cm^{-3}) for both cases: injector-pulse on and off. The operational densities were kept below this threshold to eliminate the impact of self-injection. Shown in Fig. 2 are typical e-beam spectra for the zero-delay case.

We then tuned the delay between the laser pulses. First, we scanned with large time steps (67 fs), longer than the

plasma period (35 fs for density 1.3×10^{19} cm^{-3}). Robust injection was observed in the range of delays from -850 to $+950$ fs (total of 50 plasma periods) resulting in stable quasimonoenergetic e beams with an average charge at least twice of the charge measured with the drive pulse only. Shown in Fig. 3(a) are the central energy and charge of these beams. Negative (positive) delay times correspond to the injector (drive) pulse arriving first to the intersection, see Figs. 1(a)–1(c). Based on the experimental geometry, the spatiotemporal overlap of the drive and injector pulses,
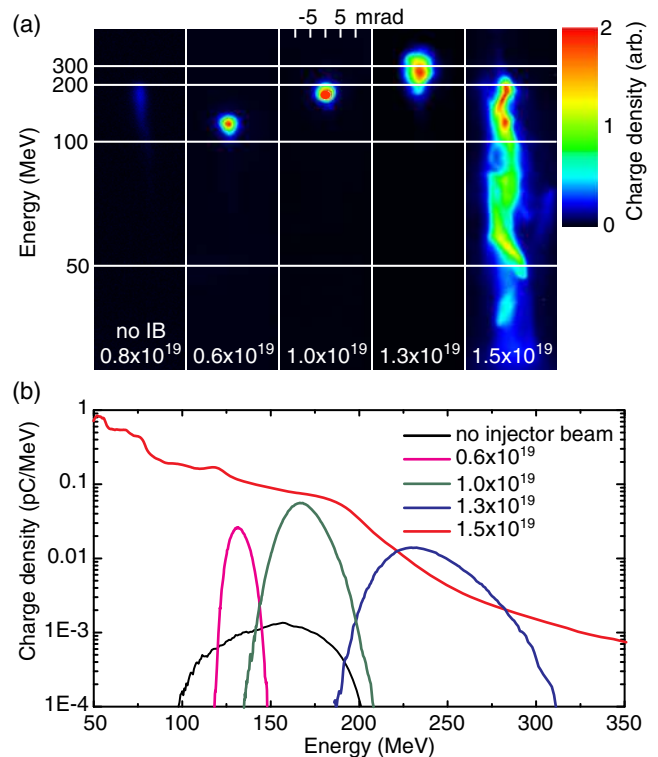

FIG. 2.   (a) Spectral profiles of magnetically dispersed e beams and (b) corresponding spectral lineouts. The left panel of (a) and the black curve in (b) show the e beam generated with the drive pulse only. The other beams were generated with both drive and injector pulses with no delay between them.
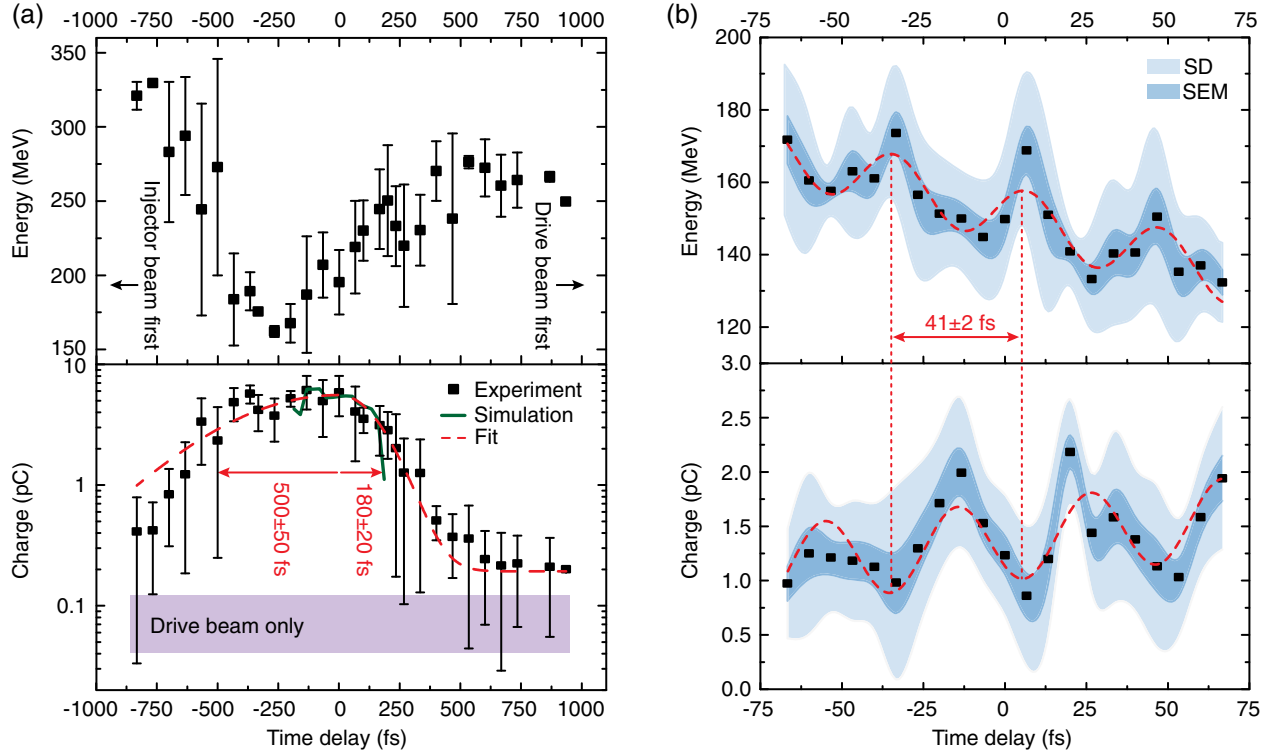
FIG. 3. Electron-beam properties vs delay between the drive and injector laser pulses. (a) Course time scan ($n_e = 1.0 \times 10^{19}$ cm^{-3}, plasma period $\tau_p = 35$ fs). Each point shows 3.4 shots on average; the error bars show standard deviations. The green line shows results of PIC simulations. Purple area shows charge measured with the drive pulse only (± 1 standard deviation). b) Fine time scan ($n_e = 7.6 \times 10^{18}$ cm^{-3}, $\tau_p = 40$ fs). Each point shows 10 shots on average. Light blue area represents standard deviation of the data, dark blue area—standard error of the mean. The red dashed lines show data fits with (a) bi-Gaussian function (red numbers show half widths at half maximum calculated from the fit); (b) sums of sine and linear functions (red number shows a period of the plasma wave, calculated from the fit).

at which they form a beat wave, and at which electrons can be injected via stochastic heating in the beat wave [22], is limited to (-200 fs; 200 fs) (see the Supplemental Material [37]). Such injection in similar delay range was observed by Plateau *et al.* [40]. Injection outside of this range, observed in our experiment, should be therefore attributed to different mechanisms. For negative delays it is wake-wake interference, for positive delays it is wake-wake interference and ponderomotive drift.

To more precisely control position within the wakefield period at which the electrons were injected, we tuned the delay between the laser pulses with a time step of 6 fs, much smaller than the plasma period (40 fs at $n_e = 7.6 \times 10^{18}$ cm^{-3}). The energy and charge of quasi-monoenergetic e beams, measured during this scan, are shown in Fig. 3(b). Both quantities exhibit oscillations, with a period (41 ± 2 fs, based on a sine fit, red lines) that closely matches the plasma period. The same oscillations were seen when the delay was scanned at twice-higher plasma density; however, the period decreased to 31 ± 5 fs, consistent with the plasma period (31 fs for 1.3×10^{19} cm^{-3}) (see Supplemental Material [37] for additional experimental and numerical modeling data). Similar oscillations were

observed in experiments on coupling of multiple laser-wakefield-acceleration stages [41]. They result from electrons being injected in different phases of the wakefield. The obvious anticorrelation of charge and energy of the e beams [Figs. 3(a) and 3(b)] can be attributed to beam loading [42]. The deviation from this pattern can be seen in the coarse scan in the range of (-250 fs; 0 fs). It can be explained by a complex host of interactions of the laser pulses and wakes. In particular, in the injector-pulse-first scenario, electrons pre-accelerated by the ponderomotive force of the injector pulse and its wake and trapped in the drive wake might go through a decelerating phase of the drive wake first and lose some energy, while in the drive-pulse-first scenario they are trapped into an accelerating phase immediately [compare Figs. 4(a) and 4(c)]. It should be noted that the trends of energy and charge on the coarse and fine-time scans can differ because they correspond to different timescales (10's of plasma periods for the coarse scan and only a few plasma periods for the fine one). Also, the scans were done at slightly different plasma densities, which translated into different dynamics of the laser pulses and their wakes, as well as the magnitude of beam loading.
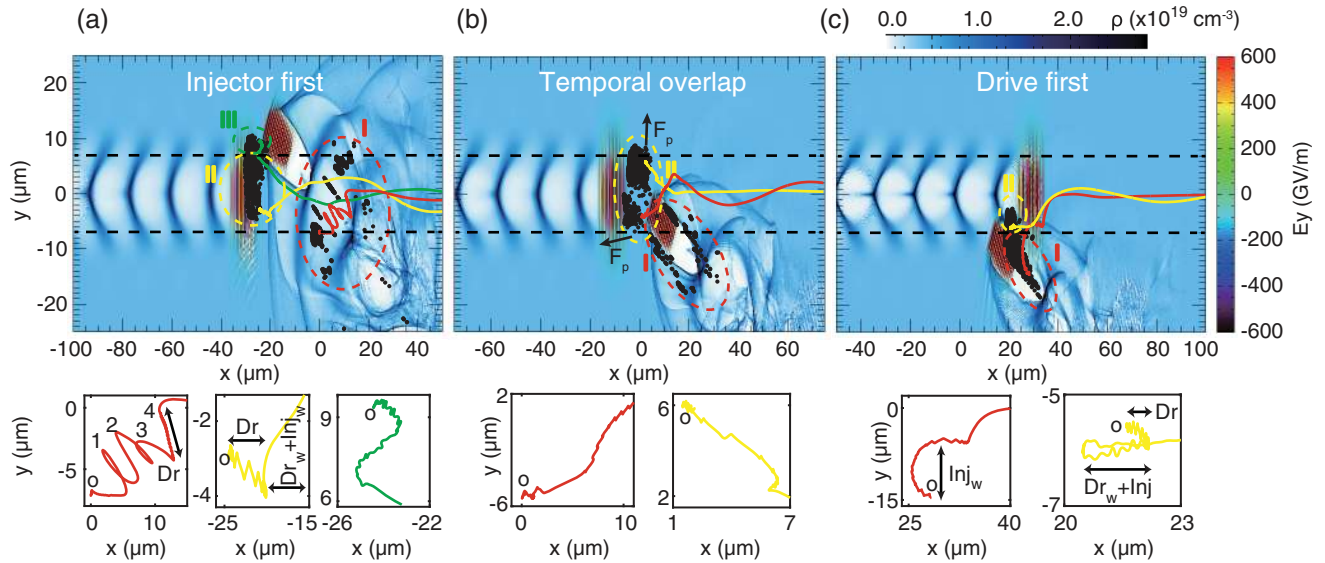
FIG. 4. Results of PIC simulations for electron injection into the drive wake in the cases when the injector pulse arrives at the intersection before the driver pulse (a), at the same time (b), or after the driver pulse (c). The white-blue-black (horizontal) color bar represents background plasma density, the red-green-black (vertical) color bar—electric field. The black points are the initial positions of typical injected electrons. The color curves show typical trajectories of those electrons. The figures at the bottom of each panel show the same trajectories with "o" marking their starting points. Labels are drive pulse (Dr), injector pulse (Inj), drive wake (Dr_w), and injector wake (Inj_w), respectively, and point to the locations along electron trajectories experiencing the field of each.

To better understand the underlying physics of the injection process, we conducted two-dimensional particle-in-cell (PIC) simulations with the code OSIRIS [43] (see Supplemental Material [37] for details). While the simulations showed injection into both drive and injector wakes, for the purposes of this Letter we focused only on electrons injected in the drive wake. When the injector pulse arrives first [Fig. 4(a)], three groups of electrons are injected. Electrons from group I originate off-axis with respect to both pulses, so they do not experience their fields directly; instead, the injector wake dominates their motion. A representative particle trajectory is shown with the red curve. The high-frequency small-amplitude oscillations are due to direct laser acceleration at the drive-laser-pulse carrier frequency. The lower frequency high-amplitude oscillations are due to the interaction with the injector wake. These electrons are injected via a wake-wake interference mechanism. Electrons in group II originate directly on the axis of the drive pulse, and to the side of the injector pulse (yellow trajectory). These electrons first experience the interaction with the drive pulse, and then are kicked and injected into the drive wakefield by the combination of the injector pulse's ponderomotive force and its wakefield [19,44,45]. This group is injected via ponderomotive drift and, partially, due to stochastic heating in the beat wave. Electrons in group III originate in front of the injector pulse (green trajectory); they experience both injector and drive pulses, as well as the fields of their wakefields [30].

When the drive and injector pulses overlap, electrons from groups I and II are injected [Fig. 4(b)]. Electrons from group II receive strong forward or backward kick (depending on their transverse positions) from the ponderomotive force of the injector pulse, which traps them into the drive wake. When the drive pulse arrives first, most charge originates from group I [Fig. 4(c)]. Those electrons are initially located on the right side of the injector pulse and experience its wakefield, which kicks them into the drive wake. Small perturbations due to interaction with injector (near the beginning) and drive (near the center) pulses can be seen on the trajectories. Electrons from group II are also located on the right side of the injector pulse, but closer to its axis.

The amount of injected charge as a function of time delay is shown in Fig. 3(a). Simulation results (green line) match well the experimental trends: the charge drops faster for the drive-pulse-first scenario than for the injector-pulse-first one. This asymmetry is clearly seen in the bi-Gaussian fit of the experimental data (red dashed line): the half width at half maximum is 180 ± 20 fs for the drive-pulse-first case and 500 ± 50 fs for the injector-pulse-first case. It can be attributed mainly to the intensity difference between the pulses. In the drive-pulse-first case, the injector's wake dominates electron trajectories at the intersection. As a result, electron acceleration along the drive-pulse direction is suppressed, and total injected charge drops quickly with increasing delay. In the injector-pulse-first case, the drive pulse collides with the injector wake, which exists for longer than the drive wake, since the injector pulse is much

stronger than the drive one. Electrons oscillating in the injector wake have sufficient energy to be trapped into the drive wake for long times (10's of plasma periods).

In the above simulations, the polarization planes of the drive and injector pulses were parallel to each other, as they were in the experiment. To study the impact of beat wave injection, we also performed a simulation with perpendicular polarizations, in which case the beat wave should not exist (see Supplemental Material [37]). The total injected charge dropped by 24% at zero delay, as compared with the parallel-polarization case, indicating that beat wave injection was not dominant, even when the drive and injector pulses overlapped.

In summary, we discussed the results of a laboratory study of wave-wave interactions in plasma. The results experimentally confirmed long-standing, but previously untested, theories of electron injection via ponderomotive drift and wake-wake interference [19,30,31]. These mechanisms are shown to produce high-quality e beams, which can be further improved by optimizing the driver-injector interaction geometry. Most importantly, precise control over the phase of the wake, at which injection takes place, is demonstrated. Such control has the potential to minimize energy spread and emittance, or increase charge, of wakefield-accelerated beams [46], whether laser-driven or charged-particle driven [20,47]. These mechanisms also have an advantage of being relatively immune to laser timing jitter and amplitude fluctuation. The accelerated electrons can reveal features of strongly nonlinear wakes that are complementary to other plasma-wave diagnostic methods used to probe linear wakes, such as ultrafast shadowgraphy [48], holography [49,50], ultrafast polarimetry [51,52], and e-beam probes [53]. We believe this new diagnostic might eventually yield further insights into nonlinear plasma phenomena, such as energy transfer with highly nonlinear plasma wakes, of interest in high-energy-density physics, astrophysics, and fusion plasmas.

*Corresponding author.
 donald.umstadter@unl.edu

[1] J. M. Laming, Astrophys. J. **546**, 1149 (2001).
[2] Z. Fan, S. Liu, and C. L. Fryer, Mon. Not. R. Astron. Soc. **406**, 1337 (2010).
[3] R. Kirkwood, J. Moody, J. Kline, E. Dewald, S. Glenzer, L. Divol, P. Michel, D. Hinkel, R. Berger, and E. Williams, Plasma Phys. Controlled Fusion **55**, 103001 (2013).
[4] A. I. Akhiezer and R. Polovin, Sov. Phys. JETP **3**, 696 (1956).
[5] T. Tajima and J. M. Dawson, Phys. Rev. Lett. **43**, 267 (1979).
[6] E. Esarey, C. Schroeder, and W. Leemans, Rev. Mod. Phys. **81**, 1229 (2009).
[7] V. Malka, Phys. Plasmas **19**, 055501 (2012).
[8] A. Rousse, K. T. Phuoc, R. Shah, A. Pukhov, E. Lefebvre, V. Malka, S. Kiselev, F. Burgy, J. P. Rousseau, D. Umstadter, and D. Hulin, Phys. Rev. Lett. **93**, 135005 (2004).
[9] F. Albert and A. G. Thomas, Plasma Phys. Controlled Fusion **58**, 103001 (2016).
[10] W. P. Leemans, A. J. Gonsalves, H. S. Mao, K. Nakamura, C. Benedetti, C. B. Schroeder, C. Tóth, J. Daniels, D. E. Mittelberger, S. S. Bulanov, J. L. Vay, C. G. R. Geddes, and E. Esarey, Phys. Rev. Lett. **113**, 245002 (2014).
[11] C. Joshi, Phys. Plasmas **14**, 055501 (2007).
[12] A. Modena, Z. Najmudin, A. E. Dangor, C. E. Clayton, K. A. Marsh, C. Joshi, V. Malka, C. B. Darrow, C. Danson, D. Neely *et al.*, Nature (London) **377**, 606 (1995).
[13] S. Banerjee, S. Y. Kalmykov, N. D. Powers, G. Golovin, V. Ramanathan, N. J. Cunningham, K. J. Brown, S. Chen, I. Ghebregziabher, and B. A. Shadwick, Phys. Rev. ST Accel. Beams **16**, 031302 (2013).
[14] S. Bulanov, N. Naumova, F. Pegoraro, and J. Sakai, Phys Rev E. **58**, R5257 (1998).
[15] S. Kalmykov, S. A. Yi, V. Khudik, and G. Shvets, Phys. Rev. Lett. **103**, 135004 (2009).
[16] J. Faure, C. Rechatin, O. Lundh, L. Ammoura, and V. Malka, Phys. Plasmas **17**, 083107 (2010).
[17] A. Pak, K. A. Marsh, S. F. Martins, W. Lu, W. B. Mori, and C. Joshi, Phys. Rev. Lett. **104**, 025003 (2010).
[18] C. McGuffey, A. G. R. Thomas, W. Schumaker, T. Matsuoka, V. Chvykov, F. J. Dollar, G. Kalintchenko, V. Yanovsky, A. Maksimchuk, K. Krushelnick *et al.*, Phys. Rev. Lett. **104**, 025004 (2010).
[19] D. Umstadter, J. K. Kim, and E. Dodd, Phys. Rev. Lett. **76**, 2073 (1996).
[20] B. Hidding, G. Pretzler, J. B. Rosenzweig, T. Königstein, D. Schiller, and D. L. Bruhwiler, Phys. Rev. Lett. **108**, 035001 (2012).
[21] M. Chen, E. Esarey, C. G. R. Geddes, E. Cormier-Michel, C. B. Schroeder, S. S. Bulanov, C. Benedetti, L. L. Yu, S. Rykovanov, D. L. Bruhwiler *et al.*, Phys. Rev. ST Accel. Beams **17**, 051303 (2014).
[22] E. Esarey, R. F. Hubbard, W. P. Leemans, A. Ting, and P. Sprangle, Phys. Rev. Lett. **79**, 2682 (1997).

[23] J. Faure, C. Rechatin, A. Norlin, A. Lifschitz, Y. Glinec, and V. Malka, Nature (London) **444,** 737 (2006).

[24] J. Faure, C. Rechatin, A. Norlin, F. Burgy, A. Tafzi, J. Rousseau, and V. Malka, Plasma Phys. Controlled Fusion **49,** B395 (2007).

[25] C. Rechatin, J. Faure, A. Ben-Ismail, J. Lim, R. Fitour, A. Specka, H. Videau, A. Tafzi, F. Burgy, and V. Malka, Phys. Rev. Lett. **102,** 164801 (2009).

[26] H. Kotaki, I. Daito, M. Kando, Y. Hayashi, K. Kawase, T. Kameshima, Y. Fukuda, T. Homma, J. Ma, L.-. Chen et al., Phys. Rev. Lett. **103,** 194803 (2009).

[27] S. Corde, K. T. Phuoc, R. Fitour, J. Faure, A. Tafzi, J. P. Goddet, V. Malka, and A. Rousse, Phys. Rev. Lett. **107,** 255003 (2011).

[28] M. Hansson, B. Aurand, H. Ekerfelt, A. Persson, and O. Lundh, Nucl. Instrum. Methods Phys. Res., Sect. A **829,** 99 (2016).

[29] J. Wenz, K. Khrennikov, A. Döpp, M. Gilljohann, H. Ding, J. Goetzfried, S. Schindler, A. Buck, J. Xu, and M. Heigoldt, arXiv:1804.05931.

[30] R. G. Hemker, K. C. Tzeng, W. B. Mori, C. E. Clayton, and T. Katsouleas, Phys. Rev. E **57,** 5920 (1998).

[31] J. R. Cary, R. Giacone, C. Nieter, and D. Bruhwiler, Phys. Plasmas **12,** 056704 (2005).

[32] G. Wittig, O. Karger, A. Knetsch, Y. Xi, A. Deng, J. Rosenzweig, D. Bruhwiler, J. Smith, G. Manahan, and Z. Sheng, Phys. Rev. ST Accel. Beams **18,** 081304 (2015).

[33] C. Liu, S. Banerjee, J. Zhang, S. Chen, K. Brown, J. Mills, N. Powers, B. Zhao, G. Golovin, and I. Ghebregziabher, SPIE LASE (International Society for Optics and Photonics, San Francisco, CA, 2013), p. 859919.

[34] W. Yan, C. Fruhling, G. Golovin, D. Haden, J. Luo, P. Zhang, B. Zhao, J. Zhang, C. Liu, M. Chen et al., Nat. Photonics **11,** 514 (2017).

[35] C. Liu, J. Zhang, S. Chen, G. Golovin, S. Banerjee, B. Zhao, N. Powers, I. Ghebregziabher, and D. Umstadter, Opt. Lett. **39,** 80 (2014).

[36] B. Zhao, J. Zhang, S. Chen, C. Liu, G. Golovin, S. Banerjee, K. Brown, J. Mills, C. Petersen, and D. Umstadter, Opt. Express **22,** 26947 (2014).

[37] See Supplemental Material at http://link.aps.org/supplemental/10.1103/PhysRevLett.121.104801 for details on the jet density profile and its measurement, which includes Ref. [38].

[38] G. Golovin, S. Banerjee, J. Zhang, S. Chen, C. Liu, B. Zhao, J. Mills, K. Brown, C. Petersen, and D. Umstadter, Appl. Opt. **54,** 3491 (2015).

[39] E. Dodd, J. Kim, and D. Umstadter, AIP Conf. Proc. **398,** 106 (1997).

[40] G. R. Plateau, C. G. R. Geddes, N. H. Matlis, E. Cormier-Michel, D. E. Mittelberger, K. Nakamura, C. B. Schroeder, E. Esarey, W. P. Leemans, S. H. Gold et al., AIP Conf. Proc. **1299,** 180 (2010).

[41] S. Steinke, J. Van Tilborg, C. Benedetti, C. Geddes, C. Schroeder, J. Daniels, K. Swanson, A. Gonsalves, K. Nakamura, and N. Matlis, Nature (London) **530,** 190 (2016).

[42] C. Rechatin, J. Faure, X. Davoine, O. Lundh, J. Lim, A. Ben-Ismail, F. Burgy, A. Tafzi, A. Lifschitz, E. Lefebvre et al., New J. Phys. **12,** 045023 (2010).

[43] R. A. Fonseca, L. O. Silva, F. S. Tsung, V. K. Decyk, W. Lu, C. Ren, W. B. Mori, S. Deng, S. Lee, T. Katsouleas et al., OSIRIS: A Three-Dimensional, Fully Relativistic Particle in Cell Code for Modeling Plasma Based Accelerators (Springer Berlin Heidelberg, 2002), Vol. 2331, p. 342.

[44] E. S. Dodd, J. K. Kim, and D. Umstadter, Phys. Rev. E **70,** 056410 (2004).

[45] V. Horný, V. Petržílka, O. Klimo, and M. Krůs, Phys. Plasmas **24,** 103125 (2017).

[46] S. Y. Kalmykov, L. M. Gorbunov, P. Mora, and G. Shvets, Phys. Plasmas **13,** 113102 (2006).

[47] R. Assmann, R. Bingham, T. Bohl, C. Bracco, B. Buttenschön, A. Butterworth, A. Caldwell, S. Chattopadhyay, S. Cipiccia, and E. Feldbaumer, Plasma Phys. Controlled Fusion **56,** 084013 (2014).

[48] M. Schwab, A. Sävert, O. Jäckel, J. Polz, M. Schnell, T. Rinck, L. Veisz, M. Möller, P. Hansinger, and G. Paulus, Appl. Phys. Lett. **103,** 191118 (2013).

[49] N. H. Matlis, S. Reed, S. S. Bulanov, V. Chvykov, G. Kalintchenko, T. Matsuoka, P. Rousseau, V. Yanovsky, A. Maksimchuk, S. Kalmykov et al., Nat. Phys. **2,** 749 (2006).

[50] P. Dong, S. A. Reed, S. A. Yi, S. Kalmykov, Z. Y. Li, G. Shvets, N. H. Matlis, C. McGuffey, S. S. Bulanov, V. Chvykov et al., New J. Phys. **12,** 045016 (2010).

[51] A. Buck, M. Nicolai, K. Schmid, C. M. S. Sears, A. Savert, J. M. Mikhailova, F. Krausz, M. C. Kaluza, and L. Veisz, Nat. Phys. **7,** 543 (2011).

[52] A. Flacco, J. Vieira, A. Lifschitz, F. Sylla, S. Kahaly, M. Veltcheva, L. Silva, and V. Malka, Nat. Phys. **11,** 409 (2015).

[53] C. J. Zhang, J. F. Hua, Y. Wan, C.-H. Pai, B. Guo, J. Zhang, Y. Ma, F. Li, Y. P. Wu, H.-H. Chu, Y. Q. Gu, X. L. Xu, W. B. Mori, C. Joshi, J. Wang, and W. Lu, Phys. Rev. Lett. **119,** 064801 (2017).